AGU PUBLICATIONS

Water Resources Research

RESEARCH ARTICLE
10.1002/2015WR017268

Key Points:
- Fines dominate attenuation at low frequency
- Single- frequency calibration possible
- Two frequency systems recover mass but not size

Correspondence to:
Y. C. Agrawal,
yogi.agrawal@SequoiaSci.com

Citation:
Agrawal, Y. C., and D. M. Hanes (2015), The implications of laser-diffraction measurements of sediment size distributions in a river to the potential use of acoustic backscatter for sediment measurements, *Water Resour. Res.*, *51*, doi:10.1002/2015WR017268.

Received 15 APR 2015
Accepted 15 OCT 2015
Accepted article online 21 OCT 2015

The implications of laser-diffraction measurements of sediment size distributions in a river to the potential use of acoustic backscatter for sediment measurements

Y. C. Agrawal[1] and D. M. Hanes[2]

[1]Sequoia Scientific, Inc., Bellevue, Washington, USA, [2]Department of Earth and Atmospheric Sciences, St. Louis University, St. Louis, Missouri, USA

Abstract We construct vertical profiles of the acoustic attenuation and back-scattering properties of a river column from measured particle concentration and size distribution profiles. The particle size and concentration data were collected in situ in the Cowlitz River in Washington, U.S., using a laser diffraction-instrument LISST-SL. The particle size distribution was bimodal, comprising a vertically well-mixed washload, and a suspended load that was similar to Rouse profiles. We then explore how well the results of converting these synthetic profiles to recover an acoustic equivalent sediment concentration and acoustic equivalent size compare with laser data in this bimodal environment. The acoustic scattering and attenuation properties are computed for four distinct frequencies: 0.5, 1, 3, and 5 MHz. It is seen that at the lowest frequency, 500 KHz, the acoustic attenuation throughout the water column is nearly constant and determined primarily by particles of size smaller than ~30 microns, i.e., the washload. At the next higher frequency, 1 MHz, the suspended load also contributed to attenuation, but even so, attenuation remained nearly constant over the vertical profile. Thus, at the two lower frequencies, attenuation was decoupled from scattering, making the inverse problem explicit for inversion. In contrast, at the two highest frequencies, scattering of sound by the suspended mode became the dominant contributor to attenuation, and attenuation varied by an order of magnitude over river depth. As for backscatter, the computed acoustic backscatter strength was determined by a combination of the washload and suspended sediment mode at all four frequencies. A fairly narrow monotonic relationship was found between total sediment concentration and locally computed backscatter, effectively providing a calibration between local backscatter signal strength and suspended sediment concentration. Such a relationship existed throughout the water column, for every frequency. The sediment concentration derived from backscatter at a pair of frequencies was within ~50% of the value measured by laser diffraction; however, the acoustic equivalent diameter exceeded the laser volume mean diameter by up to an order of magnitude. The robustness of these results for application to other flow regimes or rivers remains to be investigated.

1. Introduction

Acoustic backscatter has been used to estimate suspended sediment concentration, and sometimes size in various environments. Similar conceptually to radar and LIDAR, the idea is to transmit a pulse of energy into water and interpret the range-gated sound pressure received back at the same transducer. For example, acoustic systems with frequencies of 1–5 MHz were used by *Libicki et al*. [1989] in the deep ocean and by *Hanes et al*. [1988] in the shallow nearshore zone following the concepts described by *Hay* [1983]. With the widespread use of commercial Acoustic Doppler Current Profilers [ADCP's) operating typically at 200 KHz to 1.2 MHz, interest in extracting sediment concentration from the backscatter signal strength has grown. For example, *Gartner* [2004], and *Hoitink and Hoekstra* [2005] report using ADCP's to measure suspended sediments, mainly in the clay to silt size ranges, in coastal environments. In the past decade, several investigators report upon the use of acoustic backscatter systems to measure suspended sand in large rivers [e.g., *Topping et al*., 2007; *Wright et al*., 2010; *Guerrero et al*., 2011; *Moore et al*., 2013; *Guerrero et al*., 2013; *Latosinski et al*., 2014]. One of the more interesting topics of scientific discussion that has emerged in recent years involves the impact and importance of enhanced viscous dissipation of sound due to fine sediment in rivers [e.g., *Hanes*, 2012, 2013; *Guerrero et al*., 2014], and the publications referenced in the previous sentence]. Although the phenomenon of enhanced viscous dissipation due to small particles in water has been well known for some time [*Urick*, 1948; *Flammer*, 1962], until recently the viscous dissipation due to water and

Figure 1. Bridge-top view of the LISST-SL instrument (inset) and the site in Castle Rock, Washington. Background image is from Google Earth.

sediment had generally been ignored in acoustic interrogations of suspended sediment because the attenuation of sound due to scattering by particles was much larger than viscous attenuation. In many of the environments being investigated, such as the nearshore zone, the sediment was typically well-sorted sand. Recently, *Topping et al*. [2007] and *Wright et al*. [2010] have examined horizontal profiles in a river with the assumption of horizontal homogeneity of sediments which makes attenuation and scattering coefficients constant along the acoustic path. By assigning attenuation to fine particles and scattering to coarse ones, they solved for sediments explicitly. The validity of this approach was explained by *Hanes* [2012] who restricted it's applicability based on the relative concentrations of the fine and coarse modes. Routine inversion of vertical profiles of sediment backscatter still remains elusive, in part due to the spread of sizes and bimodality of sediment size distribution in nature. This context motivates the present work. With detailed particle size and concentration data obtained through the water column using a laser diffraction instrument, we do the forward problem first—constructing attenuation and backscatter coefficients in the water column. This examines applicability of the Topping-Wright method in a vertical nonhomogeneous profile. We then solve these synthetic scattering profiles to recover a single estimate of acoustic equivalent diameter (AED) and acoustic equivalent concentration (AEC) which we compare with the laser data. The data are from the Cowlitz river at Castle Rock, Washington, U.S. On the day of data collection, the water column had a strong Rouse like structure with a well-mixed washload and a suspended sand mode growing with depth. The laser field measurements will be described first in the following section, followed by calculations of the impact of the measured particle size distributions on acoustic properties, in turn followed by results of solving for AED and AEC in this bimodal water column.

2. Field Measurements of Sediment Size Distribution and Concentration in the Cowlitz River Using LISST-SL

A LISST-SL (**L**aser **I**n **S**itu **Scattering and Transmissometry,** -**S**tream-**L**ined), instrument was employed to profile the velocity and sediment size distribution in the Cowlitz River, at Castle Rock, Washington, U.S. (for instrument details, see http://www.sequoiasci.com/product/lisst-sl/). The instrument, shown in Figure 1, employs a pitot tube to sense river velocity and adjust an internal pump to draw in water isokinetically.

The water passes through an internal 3 mm wide test section. Multiangle laser light scattering from particles passing through this 3 mm path is measured and stored. Optical transmission across the test section is also measured to deattenuate the measured multiangle scattering. This "transmission" is similar to water turbidity. The deattenuated multiangle scattering is inverted to construct the particle size distribution (PSD).

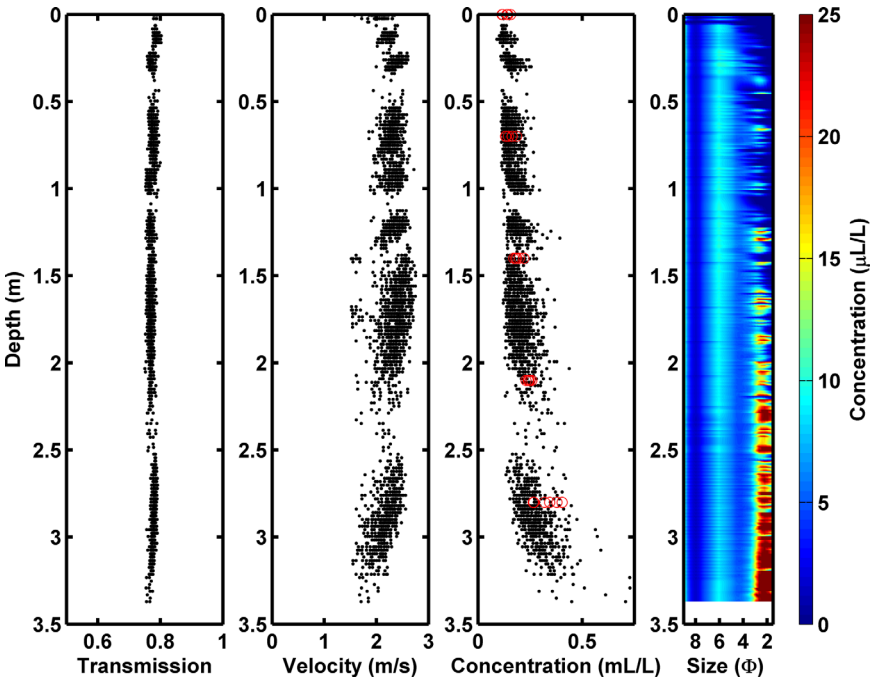

Figure 2. An overview of the data. (left to right) Optical transmission, velocity, total sediment with physical samples ('o'), and particle-size distribution.

Summing the PSD produces the total sediment concentration. This is the essence of the laser diffraction method for concentration and PSD measurement [*Agrawal and Pottsmith*, 2000]. The LISST-SL was calibrated for size and concentration fidelity in a manner identical to that used for the more widely used LISST-100X instruments. Avoiding assumptions of spherical shape of particles, the inversions employed the irregularly shaped particle model for light scattering so that the "size" reported in this paper is the sieve size [*Agrawal et al*., 2008]. Laser diffraction does not provide information on particle mass density, only volume concentrations are measured and used in this paper. *Czuba et al*. [2015] studied mass density in a survey of a number of U.S. rivers with a LISST-SL, and reported a substantially reduced "effective" density as a nationwide average. In the case of present data, for a cross comparison, USGS personnel employed P-61 samplers to grab water samples to get independent measures of mass concentrations. We have employed their mass concentrations to estimate mass density for the laser data. Only mass concentration data from these physical samples exist. At the time of this writing, P-61 samples had not been analyzed for PSD (J. Czuba and K. Spicer, USGS, personal communication, 2015), and in any case, PSD is altered in sampling and storage so that its validity is diminished in comparison to in situ data. Finally, in addition to multiangle scattering, optical transmission, velocity, water temperature, and pump control parameters were also stored with LISST-SL data.

The Cowlitz river at the bridge is approximately 200 m wide, with a straight approach of about a kilometer. The instrument was lowered from the bridge near the center of town. LISST data were collected at a bridge station 88 m from the western (river left) end of the bridge and P-61 point samples were collected at a station 100 m from the same bank, so 12 m away from the LISST. Depth at this latter station was 3.8 m throughout the duration of the experiment (K. Spicer, USGS, personal communication, 2015). The LISST-SL instrument was held steady, or lowered and raised to profile the water column over time intervals lasting between approximately 3 and 40 min. Complete size distributions and volume concentrations were measured at 2 s intervals while the instrument was being lowered and raised. A total of seven data files were obtained, containing a total of 4326 estimates of sediment concentration and size distribution. The data were acquired over a 4 h period on 14 March 2011 from 13:35 to 17:23 pm Pacific Time.

All of the LISST-SL data are shown in Figure 2, along with concentration measurements from physical samples. Optical transmission (Figure 2, first plot from left) appears constant near 80%. Velocity (Figure 2, second plot) also appears nearly constant at about 2 m/s. The concentration profile (Figure 2, third plot from

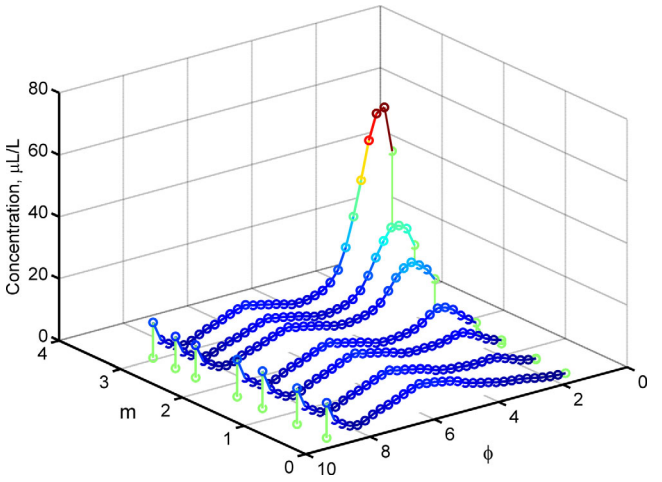

Figure 3. PSD's displayed as averages over 7 mean depths, from 0.25 to 3.25 m below surface.

left) shows a scatter of volumetric concentrations measured by LISST-SL with red circles overlaid, representing P-61 physical samples collected over the same duration. The P-61 data in this figure are converted from mass to volume using a density of 2.65 g/cm^3 for each size class. A consistent ratio of 0.88 was found in the mean volume profiles, LISST-SL vs P-61. This suggests an effective mass density for LISST-SL data of 2.33 g/cm^3 which is used for all size classes throughout the rest of this paper for computing acoustic properties. *Czuba et al*. [2015] postulate this reduced apparent density being due to flocculation, shape effects, or unmeasured size fractions. *Felix et al*. [2013], in an investigation of shape effects, confirm the accuracy of LISST measurements for randomly shaped particles. They noted that particles with preferred directions (needle-shaped quartz, platy clay) can significantly lower equivalent density. The near-unity factor of 0.88 between our data and physical samples suggests that such effects were not significant.

The data, Figure 2 (third plot), show that concentration increased from surface toward the riverbed about fourfold. At each depth, there existed a sharp and nearly uniform minimum concentration, as explained by the size distribution profile, shown in Figure 2 (far right plot). Here, a constant mode at a ϕ value of approximately 6 (16 microns) is seen. This mode is always present during the measurement period, being too fine to settle out at the high (2 m/s) river velocity. It is vertically well mixed. This is likely a washload that set the minimum concentration at all depths. Superimposed on this are particles entrained into suspension from the river bed, appearing as a scatter of points (Figure 2, third plot). These large grains appear as a mode that grows stronger with depth at ϕ value of 3 and smaller (Figure 2, fourth plot). The particle size distributions, Figure 2 (far right), averaged over seven 0.5 m thick depth segments from 0.25 to 3.25 m are shown in Figure 3. The PSD has 32 size bins, each 0.239 ϕ wide. The PSD covers a size range of 2–400 microns. In the PSD, Figure 3, a washload with a concentration $\sim$0.1 mL/L and size approximately 20 microns is clearly visible. It is consistent throughout the water column. In contrast, a sand sized sediment mode appears first at 0.75 m above bottom, and increases in prominence toward the riverbed. Note that the two points at the smallest sizes for each PSD do not represent accurate data points. The end point is set to zero to provide a visual reference for each curve, and the second point results from the total amount of light theoretically scattered by all particles smaller than the size class.

These PSD's are the essential data used in the forward problem to construct acoustic attenuation and backscatter profiles. Following a review of the relevant acoustics, the potential implications of these measured grain size distributions on acoustic properties will be explored.

3. Review of Relevant Acoustic Backscatter Principles and Methods

The theory of sound scattering from an aqueous suspension of particles and the practice of using acoustic backscatter to measure suspended sediments has been previously reviewed by *Thorne and Hanes* [2002] and updated by *Thorne and Hurther* [2014], so only a few relevant aspects are mentioned here. The typical goal is to invert the measured backscattered sound to calculate the range-dependent concentration and size of the suspended particles. The backscattered sound pressure at a transducer is the complex sum of scattering from all particles in the instantaneous ensonified volume. The particles in the ensonified volume are generally assumed to be positioned independent of each other, so that the phase of the sound wave scattered from each particle is random. The resulting sum is obtained according to incoherent scattering. As such, the net

pressure measured by a receiver is not simply the sum of the amplitudes of scattered sound waves due to individual grains, but rather it is the square root of the sum of squared amplitudes of scattering by individual grains. This is similar to some other forms of remote sensing techniques such as radar and atmospheric sonar (SODAR) both of which detect amplitudes—electric or acoustic. But it is distinct from LIDAR where the scattered light *energy* itself is detected. Also, the random phases due to individual particle scattering increase noise in the backscatter signal. Consequently, the net pressure from several sound pulses is typically averaged to obtain a statistically reliable estimate of the backscattered sound pressure.

The backscatter sound pressure for a suspension of uniform particles depends on the transmitted pulse length, $c\tau$, where c is the compressional wave speed in the water and τ is pulse duration, the transmitted pulse strength P_o at some reference range R_o, the two-way round-trip attenuation, geometrical spreading of the transmitted and backscattered sound, and the backscattering strength of the target particles. This can be written as [e.g., see *Thorne and Hanes*, 2002]:

$$P(R)=P_oR_oG_o(R)f(R)\ \{M(R)c\tau/a(R)\rho_s\}^{1/2}\exp\left(-\int 2\alpha(R)dR\right) \tag{1}$$

where the range-dependent attenuation coefficient is α, R is range, i.e., distance to the range cell from the transducer along the central path of the transmitted sound pulse, G_o accounts for combined effect of the spatial structure and spreading of the transmitted beam and received sound, f is referred to as a form factor, and M is mass concentration (dimension mass*length^{-3}) in the ensonified volume centered at range R. Sediment mass density is ρ_s (units: mass*length^{-3}) and a is particle radius.

The square of the form factor, f^2 is similar to a scattering efficiency in optics. As in optics, the acoustic scattering *intensity* is also proportional to particle area multiplied by f^2. Equation (1) can be rewritten, after absorbing $R_oG_o(R)$ and $(c\tau)^{1/2}$ into G(R) as,

$$P(R) = P_oG(R)\sigma(R)\ \exp\left(-\int 2\alpha(a,R)\ dR\right) \tag{2}$$

with

$$\sigma(R) = f(a,R)\left(M(R)/a(R)\rho_s\right)^{1/2} \tag{3}$$

and α is the total attenuation. α and σ depend upon the mass concentration of particles, their dimensionless size ka (k is $2\pi/\lambda$, and λ is wavelength), and on sediment relative density ρ_s, water temperature, and viscosity. The dimensionless form factor f depends only on ka.

It is common practice in acoustics to write equation (2) in its natural logarithmic form,

$$\ln(P(R)/P_o) = \ln[G(R)] - \int 2\alpha(R)\ dR + \ln[\sigma(R)] + N(R) \tag{4}$$

where for completeness we insert a parameter N(R), which is the signal noise floor of the instrument, but which will be ignored here on in this work.

The geometrical spreading term G(R) reduces signal strength by a fixed range-dependent amount; the specific form of G(R) depends upon the acoustic instrument system. The second term, which integrates the total attenuation over range, makes equation (4) implicit and in need of inverse methods for solution. In the general case with spatially varying sediment grain size and concentration, interpretation of backscattered sound involves two unknowns, α and σ, both representing properties of particles and water, and independent of design parameters of the instrument such as the transducer or amplifier characteristics. These parameters depend strongly on grain properties such as size and shape, and weakly upon sediment density and water viscosity for most environments. If there exists a distribution of grain sizes, then the quantities in equation (2) must be integrated over the grain size distribution such as described, for example, by *Thosteson and Hanes* [1998] or *Thorne and Meral* [2008]. Equation (2) illustrates the essential difficulty of single-frequency acoustic backscatter systems: there are two unknowns, α and σ, but only one measurement, P(R). This is in contrast with radar and LIDAR, which have the option to get an additional parameter via polarization, which does not have a counterpart in acoustics.

Two special cases arise that simplify equation (4). First, where attenuation is small due to very low sediment concentration, or short range, i.e., $\alpha R \ll \ln[G(R)]$, then the second term can be ignored and the solution of equation (4) is explicit. In the second special case, that of a homogeneous sediment suspension of concentration M (i.e., α and σ independent of R, say $\alpha = M\ \alpha_0$ and $\sigma = M^{1/2}\ \sigma_0$; where α_0 represents magnitude per unit concentration and σ_o represents magnitude per unit square root of concentration) equation (4) again becomes explicit, so that it is easily solved if α_0 and σ_0 are known. The sediment characteristic that has the greatest influence on these values in most application is size. In this case, the constant term $-2M\alpha_o R$, adds to ln[G(R)], together determining the slope whereas the scattering term sets an offset in equation (4). G(R) being known, the excess attenuation due to sediment can be read graphically from the excess slope of data plotted as signal strength versus range, yielding $-2M\alpha_o R$; and the offset yields $\ln(M^{1/2}\ \sigma_0)$, equation (3). This is the method employed by *Topping et al*. [2007] and *Wright et al*. [2010]. They made the further assumption that attenuation was dominated by fine grains, so that the slope term yielded concentration of fine grains, with an assumed size. Similarly, the offset was assigned to coarse grains, so that the offset yielded coarse grain concentration, also with assumed grain size for sand. *Hanes* [2012] explained their success by decomposing M into two components, M_1 for fines that produce attenuation, and M_2 for coarse that produce scattering. *Hanes* [2012] defined the region of validity of the method of *Topping et al*. [2007] and *Wright et al*. [2010] in terms of the relative attenuation and scattering of the two components. We apply the *Hanes* [2012] criteria to comment on their applicability to the present data.

We now consider the forms of α and σ. *Urick* [1948] and *Flammer* [1962] showed that the attenuation of sound due to small particles suspended in a viscous fluid has two contributing mechanisms. First is viscous dissipation due to shear produced by the relative motions of particles and the fluid oscillating in the sound wave pressure field. The second mechanism is scattering attenuation where energy is lost to the acoustic beam by the scattering of incident waves out of the incident beam. Both these mechanisms act in addition to the viscous dissipation due to the movement of the clear fluid in response to the sound wave pressure field. The various attenuation mechanisms are additive such that:

$$\alpha = \alpha_w + \alpha_{sv} + \alpha_{ss} \tag{5}$$

where α_w is the viscous attenuation due to clear water, α_{sv} is the viscous attenuation due to sediment, and α_{ss} is the scattering attenuation. For larger particles, the viscous attenuation becomes negligible, and the dominant scattering attenuation becomes proportional to the total cross-sectional area of the particles (just like optical scattering). The viscous attenuation due to particles depends in part on the ratio of the acoustic frequency to fluid kinematic viscosity, and therefore does not reduce to a dimensionless function of *ka* alone. The scattering attenuation term has been expressed by semiempirically best-fit formulae as a dimensionless function of *ka* alone by a number of authors (e.g., *Thorne and Hurther* [2014], equation ((3)b), or *Moate and Thorne* [2012], equation (12) and Table 4 for various mineral grains). *Hanes* [2012] Figure 1a shows the dependence of α_{sv} [following *Urick*, 1948] and α_{ss} [following *Thorne and Hanes*, 2002] as a function of *ka* and mass density of 2.65 g/cc, for acoustic frequencies of 0.2, 1.0, and 5.0 MHz. These are expressed in the figure as Nepers/cm/C, but are sometimes expressed in a normalized form of 1/length, or in units as mass/length^2. Both the viscous attenuation and the scattering attenuation for a fixed volume concentration first increases and then decreases with increasing *ka*, but the scattering attenuation peaks at a much larger value of *ka* than the viscous attenuation. This combined attenuation therefore has a minimum value around $ka = 0.2$–0.4 for these acoustic frequencies and typical values of water kinematic viscosity.

In the calculations that follow, we use the formula due to *Urick* [1948] for the viscous dissipation due to particles of diameter D in fluid, normalized by mass:

$$\alpha_{sv} = \left[\frac{k}{2\rho_s}(\sigma-1)^2\left(\frac{s}{s^2+(\sigma+T)^2}\right)\right] \tag{6}$$

where $\sigma = \rho_s/\rho_f, \rho_f$ and ρ_s are fluid and sediment density, $s = \frac{9}{2\gamma D}\left(1+\frac{2}{\gamma D}\right)$, $\gamma = \sqrt{\pi F/\nu}$, F is the frequency of the backscatter system, ν is kinematic viscosity of the fluid, and $T = \frac{1}{2} + \frac{9}{2\gamma D}$. The parameter γ represents the inverse viscous diffusion distance of the boundary layer on a particle, forced by the oscillating motion of waves. For scattering loss, we use the equations suggested for distributions of natural sand by *Thorne and Meral* [2008], where $x = ka$:

$$\alpha_{ss}=\left[\frac{1.5}{D\rho_s}\left(\frac{0.29x^4}{0.95+1.28x^2+0.25x^4}\right)\right] \tag{7}$$

The backscattering of sound described in equation (3) depends on the mass concentration of suspended sediments, M, grain size, a, and particle mass density, ρ_s. M/ ρ_s a is the area concentration, so the scattering depends on the form factor f times the square root of area concentration, or for fixed grain size and density, on square root of mass concentration. It is useful here to note that similar to radar and LIDAR, acoustic backscattering spans the Rayleigh region ($ka \ll 1$), a transition region ($ka \sim 1$), and the geometric region ($ka \gg 1$). Correspondingly, f scales as $(ka)^2$ in the Rayleigh region, and asymptotes to 1.1 for $ka \gg 1$. As mentioned above, the backscatter form function, f, has been semiempirically fit to measurements using natural sand by several researchers. We use the following formula for f [e.g., *Thorne and Hanes*, 2002]:

$$f=1.1\left\{1-0.25\exp\left[-\left(\frac{x-1.4}{0.5}\right)^2\right]\right\}\left\{1+0.37\exp\left[-\left(\frac{x-2.8}{2.2}\right)^2\right]\right\}\left\{\frac{1.1x^2}{1+1.1x^2}\right\} \tag{8}$$

We next consider a *distribution* of particle sizes in water, which is the more common natural condition. For distributions of sediment at concentrations sufficiently low to avoid particle-particle interactions, the total attenuation α_T from a distribution of particle sizes is additive:

$$\alpha_T=\sum\nolimits_i \alpha_i \tag{9}$$

where α_i represents the total attenuation due to the concentration of suspended sediment within a narrow size class denoted by i. The size classes of the LISST-SL are $\sim 1/4\ \phi$ wide, so we treat them as single sizes.

In contrast to the attenuation coefficient, the total backscatter is calculated as the square root of the sum of squared backscatter due to individual size classes:

$$\sigma_T=\left[\sum\nolimits_i \{f^2 M/(\rho_s a)\}_i\right]^{1/2} \tag{10}$$

where all parameters in curly brackets vary with the size class i. The presence of f^2 in equation (10) is significant as it diminishes the contribution to backscattering by small particles in the Rayleigh regime (for which $f^2 \ll 1$) relative to large particles, which may be in the geometric scattering regime.

As a prelude to the discussion of results reported in this paper, we close this introduction with a brief review of methods to invert the backscatter measurement for extracting a characteristic particle size and sediment concentration at each range bin, which we refer to below as unknowns. The solution seeks a range-varying acoustic equivalent mass concentration, M_A, and an acoustic equivalent particle diameter, D_{AE}. Since the problem is underdetermined (more unknowns than data), a concentration profile $M_{A,1}$ can be found to exist for any assumed size, so that a solution surface $M_{A,1}(D_{AE}, R)$ in the size-range space can be constructed. Any point on this surface represents a possible solution. If a second frequency signal is available, a second solution surface $M_{A,2}$ (D_{AE}, R) can be produced. The intersection of these two surfaces constitutes the solution of M_A and D_{AE}, as functions of R. The solution can only describe the mass concentration and diameter corresponding to a *single equivalent* size versus range, even when a distribution of sediment sizes exists in reality. Adding more acoustic frequencies permits construction of more such solution surfaces. Any pair of surfaces provides a solution for D_{AE} and M_A. Due to the nonlinear relationship between scattering and grain size, equation (3), when a distribution of sizes is present, no simple relationship exists between D_{AE} and the actual size distribution in nature. For example, in a broad size distribution or a bimodal situation, the recovered D_{AE} from different frequency pairs may not match. Indeed, we show this to be the case later. We have mentioned the work of *Topping et al.* [2007] and *Wright et al.* [2010]. Their work was with a single frequency, side-looking system so that their insight in assigning attenuation to fines and scattering to coarse grains was key to invert data. The side-looking profile makes the sediment field homogeneous. In another notable effort, *Moore et al.* [2013] inverted attenuation estimates alone from a multifrequency system with varying degree of success when compared with synthetic values from particle size data with a laser diffraction instrument. They did not attempt inverting a vertical profile. Recently, *Latosinski et al.* [2014] reported inverting for vertical profiles, but they too assumed vertically homogeneous, *known* size sediment. Assuming one of two parameters renders the intractable problem of equation (2) tractable.

It is worth noting here that there are many ways to characterize a distribution of grains, e.g., by number density, area, or volume distribution. Care needs to be exercised in specifying which mean diameter is relevant.

Different technologies often produce inconsistent results also. For example, it is common for geologists to compute a geometric mean grain diameter based upon the weight of the grains. This has been typically accomplished by sieving grains through a series of rectangular mesh sizes, weighing the amount of material in each sieve, converting the measurements onto a logarithmic (e.g., ϕ) size scale, and graphically or computationally estimating the arithmetic mean of the weight-log(size) distribution. This method is subject to bias due to the manner in which irregular shaped particles sift through a rectangular mesh, and also due to density differences between particles. Laser diffraction, on the other hand, estimates volume concentrations in narrow size classes from measurements of laser light scattering into correspondingly multiple narrow angles. Since the size classes are narrow, the area distribution, or number density of particles in these narrow size bins can also be extracted from the volume distribution, so that a number-mean, or area-mean size can also be extracted. The laser diffraction method does, however, have a limitation of a predefined size range, so that it excludes particles outside this size range. However, for the present purpose, any bias introduced by this omission is not of consequence, since the comparison in this paper will be between laser data and acoustic properties derived from this same laser data. In that regard, such a comparison could as well be done purely with synthetic data. Field data make the comparison realistic and relevant. Now, the single characteristic size determined for a distribution of grains using acoustic backscatter is a complex function of the PSD, equation (10). So, the mean size measured by acoustic backscatter is neither a number mean, nor an area or volume mean size. That does present a conceptual difficulty while comparing an equivalent acoustic size D_{AE} with a volume mean size defined, in this case, by the laser diffraction technique.

The vertical distribution of sediments in a river shows gradients in both size and concentration, such as were shown in Figure 3 for the Cowlitz River. In flows that are vigorous enough to suspend bed material, a vertical sediment concentration profile exists with higher concentrations near the river bed, decreasing upward. This is an environment not only of vertically changing concentration but also of changing mean size. How does this condition affect acoustic backscatter and attenuation? That is the question addressed in this paper. We have used data on particle size *distribution* and its vertical *profile* to compute the profiles of attenuation α and backscattering coefficient σ, and from the latter at pairs of frequencies, solved for the acoustic equivalent concentration and diameter, M_A and $D_{AE.}$ We then contrast these solutions with LISST-SL measurements. Of particular interest, in light of *Topping et al*. [2007], *Wright et al*. [2010], and *Hanes* [2012], is the question if their criteria were satisfied for some frequencies in this bimodal river profile, so that their method may be applicable in this river also, at least on some occasions.

4. Calculations of Acoustic Scattering and Attenuation

Using equations (4)–(10), we next compute the contributions to total attenuation and backscattering coefficients from each of the 32 size classes in the PSD measured by LISST-SL. The attenuation is shown in Figure 4 as cumulative values. Each line represents the integration from the minimum diameter (smallest size bin of laser) to the current diameter (abscissa), for a single point on Figure 2 (third plot). The LISST-SL data contain 32 size bins, so that a single size-distribution measurement (i.e., one point out of 4326 shown in Figure 2) results in one cumulative curve for α (and one for σ). The cumulative attenuation plots, Figures 4a–4d show the growth of the total attenuation from contributions by increasing grain sizes. At the lowest frequency, 0.5 MHz, attenuation reaches its full value essentially at about 30 microns, i.e., larger particles do not add significantly to the total attenuation *anywhere* in the water column. In other words, at 0.5 MHz attenuation is indeed governed entirely by fine particles throughout the water column. This situation conforms with one of the *Topping et al*. [2007] assumptions. In contrast, at higher frequencies, an increasing part of the size spectrum contributes to the total attenuation. At 1 MHz, contribution from grains $>$200 microns increases attenuation by 2–3 times compared to its magnitude at river surface. At 3 and 5 MHz, the sand fraction ($>$100 micron) increases attenuation by well over an order of magnitude compared to contribution of particles below 30 microns. It follows that the assumption of a vertically constant attenuation, determined solely by fine particles, does not apply in this water column for the three higher frequencies.

We next explore the similar issue of contribution from different parts of the size spectrum to backscatter, σ. This is shown in Figure 5, in the same order of frequencies as Figure 4. The cumulative value is now calculated consistent with incoherent scattering, i.e., following equation (11),

σ_n the scattering coefficient up to size class *n* is:

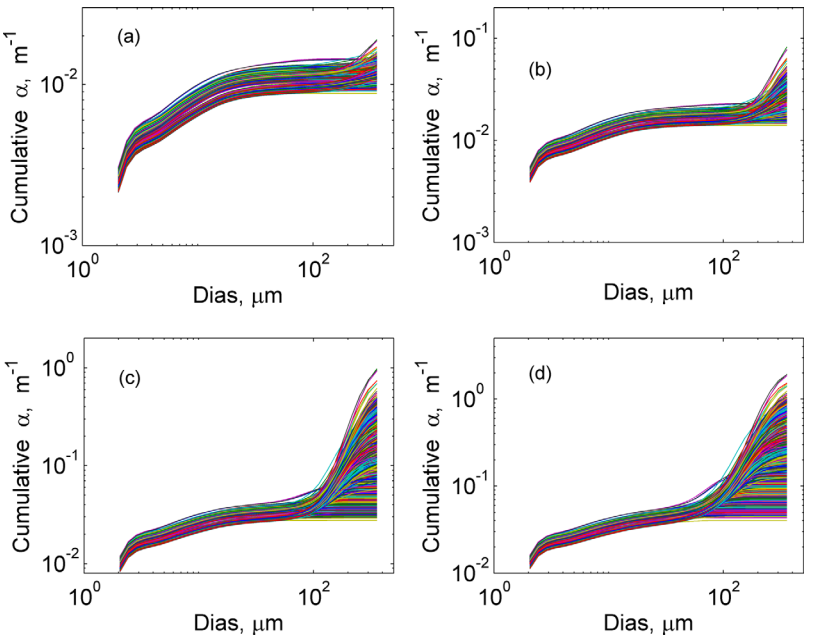

Figure 4. Cumulative attenuation (due to particles alone, not including clear water viscous attenuation), a, b, c, and d, respectively, 0.5, 1, 3, and 5 MHz.

$$\sigma_n = \left[\sum^{n}\{f^2[M/(\rho a)]\}_i\right]^{1/2} \tag{11}$$

where the summation over the index *i* is from size classes 1 to *n*.

It is seen that the value of σ is determined by contributions from all parts of the particle size spectrum, for all four frequencies. At the surface, in all four cases, the cumulative σ curves flatten out at ~30 microns when no coarse grains are present at the surface. However when coarse particles appear, σ increases by an order of magnitude for all four frequencies. So, whereas fines governed attenuation at 500 kHz, backscatter

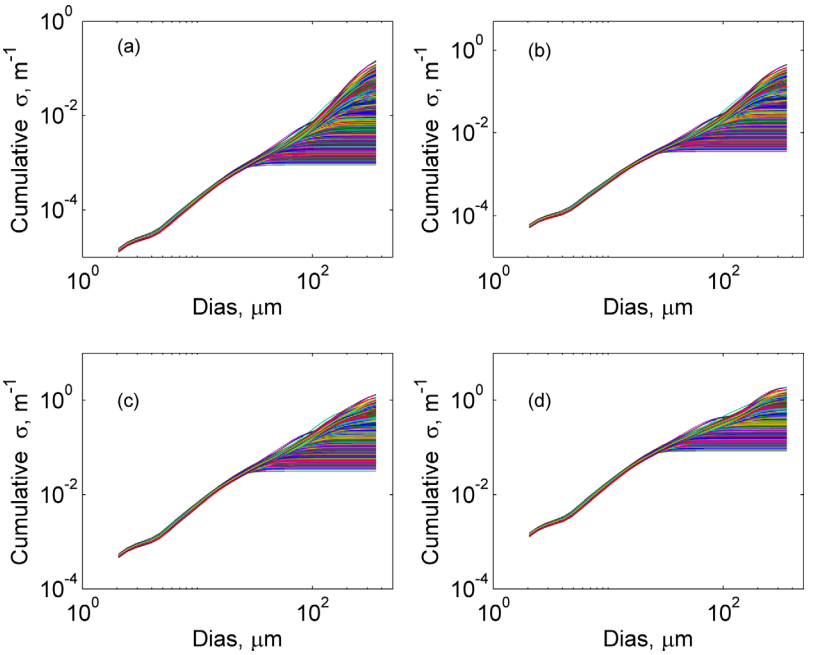

Figure 5. The backscatter at the four frequencies. Figure plots are in same order as in Figure 4.

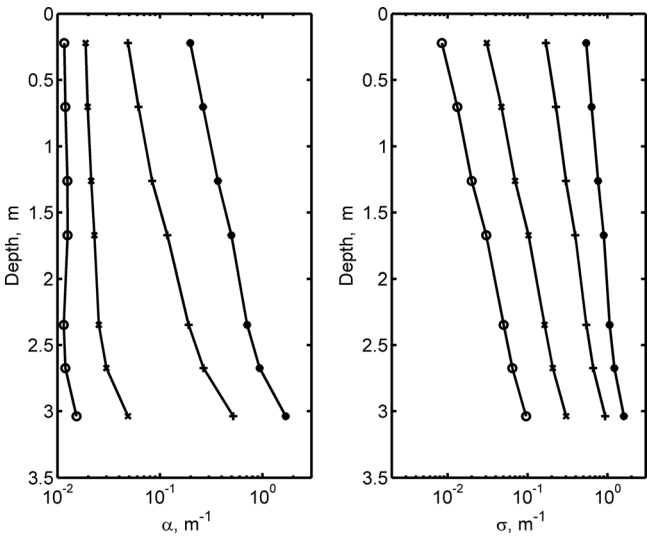

Figure 6. Vertical profiles of the (left) attenuation and (right) scattering. The four lines each represent a frequency: circle: 0.5 MHz, cross: 1 MHz, plus: 3 MHz, and asterisk: 5 MHz. The symbols show where mean values are computed.

is not governed by coarse particles alone. Near the surface, σ is determined by the washload. In other words, the simplification of horizontally homogeneous suspension—sands control σ—exploited by *Topping et al.* [2007] cannot be used in this vertically inhomogeneous river column. Backscatter is now depth dependent, more complex to interpret.

We next display the vertical variation in total attenuation and backscatter, averaged in 0.5 m depth bins, in Figure 6, similar to what an acoustic system would encounter. Both parameters show a steady increase toward the bottom, but there are qualitative differences. Attenuation is nearly constant vertically for the two lower frequencies, and $2\alpha R \ll 1$ even at maximum depth, R = 3.5 m. Backscatter, on the other hand, increases from top to bottom consistently by about an order of magnitude for all frequencies.

The data of Figures 4 and 5 are the essence of the results condensed from field data on particle size distributions. It emerges that attenuation being constant, with its magnitude set by fines alone applies at 0.5 MHz, and by inference, at lower frequencies. This parallels the case of side-looking single-frequency acoustic backscatter measurements. However, backscatter does not depend on coarse grains alone, thus thwarting the possibility of assigning backscatter to a single-size sand fraction. In short, the conditions defined by *Hanes* [2012] to apply the Topping-Wright model are only partially applicable for these data.

It remains to explore if the backscatter from any depth cell is uniquely and monotonically related to the suspended sediment concentration. If this holds true, then a calibrated, single-frequency backscatter system could measure the suspended sediment concentration once adjusted for attenuation. The backscatter-concentration relationship is shown in Figure 7 (left) for the four frequencies. At low concentrations where washload is dominant part of the total, the relationship is nearly log-linear, continuing out to higher concentrations but with a reduced slope, associated with the rise of the coarse mode. Figure 7 (right) shows the same relationship in a linear plot for 500 kHz. The existence of a narrowly defined, depth-independent relationship between σ and concentration is encouraging. Its existence was not anticipated in this variable PSD environment. These curves serve as a size-corrected calibration for backscatter, so that once correction for attenuation is made, concentration can be extracted within reasonably narrow error band. In other words,

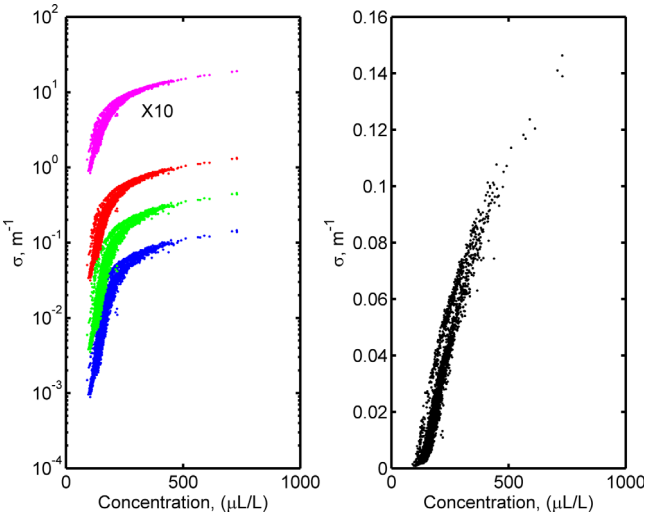

Figure 7. Relationship of total sediment concentration and backscatter throughout the (left) water column for all frequencies (from bottom upward: 0.5,1, 3, 5 MHz); the 5 MHz values are amplified by a factor of 10 (shifted upward) for improved visibility; (right) 0.5MHz alone. Each data point corresponds to a data point in Figure 2 (third plot).

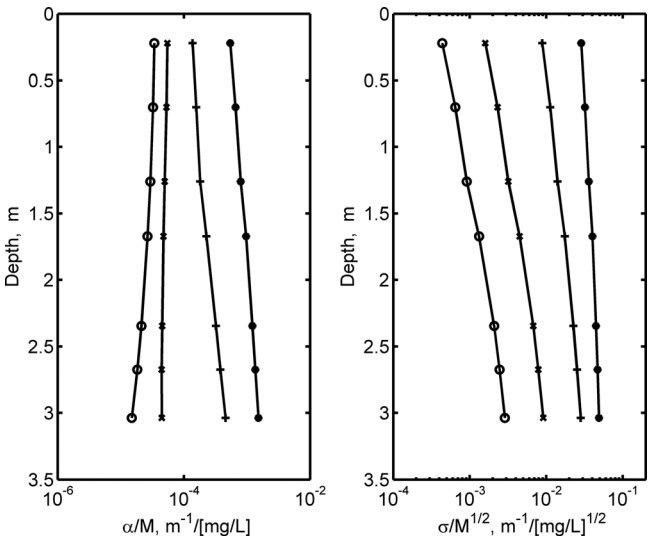

Figure 8. Vertical profiles of α normalized by total suspended concentration M, and σ normalized by $M^{1/2}$. Symbols are same as Figure 6.

the second condition of *Hanes* [2012], while not applicable, can be ignored, and concentration from a single-frequency system can be extracted from this calibration for the specific conditions prevailing at the time of this experiment.

As a final view of this data, Figure 8 shows recomputed attenuation and scattering coefficients normalized, respectively, by the mass concentration and its square root, following equations (9) and (10). This serves as a sort of calibration that differs from the homogeneous suspension case. It shows the variability in α and σ due solely to variations in the size distribution of the suspended sediments (in a homogeneous or single-size suspension, this normalization would render the profiles of α/M and $\sigma/M^{1/2}$ constant). When attenuation is dominated by fines, i.e., the 0.5 MHz case, the attenuation per unit mass actually decreases toward the riverbed by about a factor of 2. The magnitude of α/M increases only mildly for 1 MHz but increases by approximately a factor of 4 between the water surface and the riverbed for 3 and 5 MHz. This is due to large grains making increasingly more important contribution to the total attenuation, as shown previously in Figure 4. The order of magnitude change in $\sigma/M^{1/2}$ (Figure 4, right plot), implies a greater scattering per unit mass at depth, reflecting the higher form factor *f* for larger grains. It also indicates that ignoring grain size changes will cause serious error in interpreting σ.

5. Calculating M_A and D_{AE} Solely From Backscatter at Frequency Pairs

It is interesting to explore how a single characteristic sediment size, and concentration, derived from multi-frequency measurements compares to the volume mean size measured with the laser. This direct solution of the backscatter estimates at frequency pairs represent the most conservative (i.e., least accurate) estimate that can be obtained for D_{AE}, and $M_{A,}$ because only two frequencies are employed, and no information is assumed regarding the shape of the actual PSD. Although such an approach was used by *Jourdin et al.* [2014] with some success, it should be clarified here that one would generally not use this approach in practice; rather information or assumptions about the PSD (ala *Moate and Thorne* [2009] and others), and additional frequencies would typically be employed to improve the estimates.

D_{AE}, and M_A can be computed from any two frequencies, via:

$$\sigma_1 = f_1[2M_A/D_{AE}\rho_s]^{1/2}, \text{ and}$$
$$\sigma_2 = f_2[2M_A/D_{AE}\rho_s]^{1/2}. \tag{12}$$

The solution is found graphically by constructing two lines, using two backscatter estimates:

$$M_A = D_{AE}\rho_s \ \sigma_1^2/2f_1(D_{AE}), \text{ and}$$
$$M_A = D_{AE}\rho_s \ \sigma_2^2/2f_2(D_{AE}) \tag{13}$$

for a range of single sizes from 1 to 500 microns, and the intersection point determines M_A and D_{AE}. In Figure 9, we show D_{AE} contrasted with the volume mean diameter (VMD) computed from the laser measurements, and M_A normalized by the concentration M measured by laser. VMD is derived from PSD. The size bins of the LISST-SL are logarithmic, so that the *i*th size is related to the minimum size D_o as $D_i = D_o r^i$. For

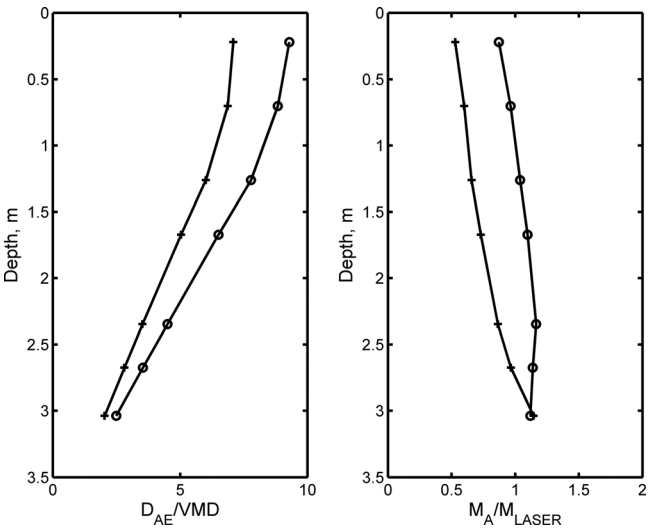

Figure 9. (left) Acoustic equivalent diameter D_{AE} normalized with laser estimated VMD; and, (right) acoustically estimated concentration, M_A, normalized by laser estimate, M_{LASER}. Circle: 0.5 and 1 MHz; plus: 0.5 and 3 MHz.

LISST-SL, $D_o = 2.06$ μm, and $r = 1.1801$. The size bin of the mean diameter is computed from first moment, where the summation is over 32 size classes:

$$I = \sum_i iV_i / \sum_i V_i; \text{ and} \quad (14a)$$

$$\text{VMD} = D_o r^I \quad (14b)$$

We show these results using two pairs of frequencies: 0.5 and 1 MHz and 0.5 and 3MHz. It is seen that M_A is within 50% of the laser estimate, whereas the D_{AE} departs from the VMD by nearly an order of magnitude when fines dominate near the surface, but reaches within about a factor of 2 of the VMD when coarse grains dominate the size distribution near the riverbed. The two frequency pairs also give somewhat disparate results.

Finally, for conceptual purposes, we briefly present the scattering target strengths of different size sediment grains on a per unit mass basis, and at these four frequencies. This illustrates relative sensitivity to grain size in a polydispersion. Recall that due to random phases of the scattering particles, their contributions add linearly to the scattered sound *intensity*, i.e., sum of pressure squared. Thus, to see relative contribution of different size classes, it is important to compare the scattering *intensity* of each size class, i.e., P^2_{rms}.

The scattering intensity of a size class is proportional to f^2 times the area concentration. The weight of each size class, from equation (9), is:

$$\sigma_i^2 = [f^2/(\rho_s a)]_i M_i; \quad (15)$$

or, rewriting

$$\sigma_i^2 = w_i M_i; \text{ where} \quad (16)$$

$$w_i = [f^2/(\rho_s a)]_i \quad (17)$$

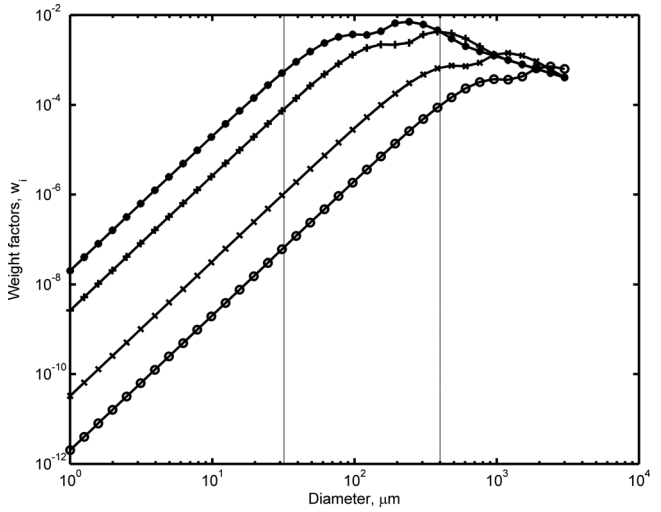

Figure 10. The weight factors w_i of equation (16) versus diameter ($D = 2a$) (symbols follow Figure 6). The two vertical lines define (left) washload, and (right) upper measured sizes of LISST-SL. Note the $1/D^{1/2}$ type decline for large *ka*, which follows from equation (17) with *f* reaching an asymptotic value of 1.1 for large particles. In the Rayleigh regime ($ka \ll 1$), $w_i \sim D^3$.

In other words, the contribution to acoustic backscatter *intensity* from any size class, on a per unit mass basis is proportional to a weight factor specifically applicable to that size, w_i. The weight factors w_i from equation (15) are shown in Figure 10, with $\rho_s$set equal to 2.65 gm/cc. It is obvious that fine particles are weighted very low, and hence do not influence the total scattering σ in the presence of even a small mass of coarse grains. These curves show the Rayleigh relationship for $ka \ll 1$, where w_i varies as a^3, and then declining as $1/a$ for $ka \gg 1$ in the geometric scattering regime. These weight factors effectively serve as

filters—sensing large grains preferentially. It is this behavior that renders the concentration—σ relationship so strongly dependent on the larger grains in the Rayleigh regime, but much less so in the Mie regime.

6. Conclusions

This paper was motivated by the opportunity to explore the acoustic attenuation and scattering properties of the water column with a rich, incidental data on sediment size distributions in a river. The remarkable success of *Topping et al*. [2007] and *Wright et al*. [2010], explained in part by *Hanes* [2012], in extracting size and concentration along a horizontal line of sight with a single-frequency acoustic Doppler system begged the question: would it work in a water column, and how well?

Hanes [2012] considered an idealized uniform suspension with just two widely different particle sizes. He showed that two conditions must be satisfied in order for the attenuation and backscatter to be decoupled from each other, governed, respectively, by fine and coarse fractions:

$$\text{Attenuation}: \quad \alpha_1 M_1 >> \alpha_2 M_2 \tag{18}$$

$$\text{Scattering}: \quad f_2^2 [M/(\rho_s a)]_2 >> f_1^2 [M/(\rho_s a)]_1 \tag{19}$$

where the subscript 1 indicates the smaller size sediment and subscript 2 indicates the coarser. It is evident from Figures 4 and 5 that the attenuation condition, equation (18) is satisfied for the present data at the two lower frequencies, for this bimodal PSD, spanning 2–400 micron grains. The scattering condition, however, equation (19) is generally not satisfied for these data. If the PSD were constant, variations in concentration alone would still yield a linear relationship between $M^{1/2}$ and σ. Instead of this relationship, and despite variations of the grain size distribution with depth, an unexpected and fairly tight relationship between total concentration and total backscatter was found throughout the water column for all frequencies, as shown in Figure 7. This suggests that independently measured profiles for concentration normalized α and σ, such as those shown in Figure 8, could be used in lieu of PSD information in standard inversion methods to obtain concentration profiles from a single-frequency acoustic backscatter system, but only if the vertical PSD profile remains similar over the duration of the measurements.

The success of such a strategy to recover sediment concentration in a bimodal vertical column thus depends on the existence of a robust relationship between concentration and backscatter in addition to acoustic calibration of any particular instrument. How does the M-σ relationship shown in Figure 7 or the curves such as shown in Figure 8 change over time with, for example, a change in river velocity or sediment supply? Velocity-dependent relationships for attenuation and scattering may well be fairly stable for a particular river, although the sediment response to currents is generally much more complex, with variable time lags and nonuniqueness. If two or more frequencies are available, and the instruments are calibrated for their acoustic and electronic parameters so that, backscatter and attenuation are accurately measured, then even in bimodal size distributions and a nonhomogeneous water column, concentration can be extracted reasonably. The acoustic equivalent size estimates calculated assuming a single representative particle size has substantial error, much as expected, in contrast to single-mode PSD's such as those reported by *Hay and Sheng* [1992] for narrow size distributions, and *Moate and Thorne* [2009] for broad size distributions.

Acknowledgments
We would like to acknowledge Chris Curran and Kurt Spicer, USGS, Tacoma, Washington for permission to use their data. Y.C.A. was supported by internal R&D funds of Sequoia Scientific. D.M.H. acknowledges the support of Saint Louis University. The data used in this paper may be obtained from Y.C.A.

References

Agrawal, Y. C., and H. C. Pottsmith (2000), Instruments for particle size and settling velocity observations in sediment transport, *Mar. Geol.*, *168*(1–4), 89–114.

Agrawal, Y. C., A. Whitmire, O. A. Mikkelsen, and H. C. Pottsmith (2008), Light scattering by random shaped particles and consequences on measuring suspended sediments by laser diffraction, *J. Geophys. Res.*, *113*, C04023, doi:10.1029/2007JC004403.

Czuba, J. A., T. D. Straub, C. A. Curran, M. N. Landers, and M. M. Domanski (2015), Comparison of fluvial suspended-sediment concentrations and particle-size distributions measured with in-stream laser diffraction and in physical samples, *Water Resour. Res.*, *51*, 320–340, doi: 10.1002/2014WR015697.

Felix, D, I. Albayrak, and R. M. Boes (2013), Laboratory investigation on measuring suspended sediment by portable laser diffractometer (LISST) focusing on particle shape, *Geomar. Lett.*, *33*, 485–498, doi:10.1007/s00367-013-0343-1.

Flammer, G. H. (1962), Ultrasonic measurement of suspended sediment, *U.S. Geol. Surv. Bull.*, *1141-A*, 48 pp.

Gartner, J. W. (2004), Estimating suspended solids concentrations from backscatter intensity measured by acoustic Doppler current profiler in San Francisco Bay, California, *Mar. Geol.*, *211*, 169–187.

Guerrero, M., R. Szupainy, and M. Amsler (2011), Comparison of acoustic backscattering techniques for suspended sediments investigation, *Flow Meas. Instrum.*, *22*(5), 392–401.

Guerrero, M., R. N. Szupiany, and F. Latosinski (2013), Multi-frequency acoustics for suspended sediment studies: An application in the Parana River, *J. Hydraul. Res.*, *51*(6), 696–707.
Guerrero, M., N. Ruther, and R. Archetti (2014), Comparison under controlled conditions between multi-frequency ADCP's and LISST-SL for investigating suspended sand in rivers, *Flow Meas. Instrum.*, *37*, 73–82.
Hanes, D. (2012), On the possibility of single frequency acoustic measurement of sand and clay concentrations in uniform suspensions, *Cont. Shelf Res.*, *46*, 64–82, doi:10.1016/j.csr.2011.10.008.
Hanes, D. M. (2013) Erratum to "On the possibility of single-frequency acoustic measurement of sand and clay concentrations in uniform suspensions", *Cont. Shelf Res.*, doi:10.1016/j.csr.2012.10.003.
Hanes, D. M., C. E. Vincent, D. A. Huntley, and T. E. Clarke (1988), Acoustic measurements of suspended sand concentration in the Canadian Coastal Sediment Study experiment at Stanhope Lane, Prince Edward Island, *Mar. Geol.*, *81*(1), 185–196.
Hay, A. E. (1983), On the remote acoustic detection of suspended sediments at long wavelengths, *J. Geophys. Res.*, *88*(C12), 7525–7542.
Hay, A. E., and J. Sheng (1992), Vertical profiles of suspended sand concentrations and size from multi-frequency acoustic backscatter, *J. Geophys. Res.*, *97*(C12), 15,661–15,677.
Hoitink, A. J. F., and P. Hoekstra (2005), Observations of suspended sediment from ADCP and OBS measurements in a mud-dominated environment, *Coastal Eng.*, *52*, 103–118.
Jourdin, F., C. Tessier, P. Le Hir, R. Verney, M. Lunven, S, Loyer, A. Lusven, J. Filipot, and J. Lepesqueur (2014), Dual-frequency ADCPs measuring turbidity, *Geo Mar. Lett.*, *34*, 381–397.
Latosinski, F. G., R. N. Szupiany, C. M. Garcia, M. Guerrero, and M. L. Amsler (2014), Estimation of concentration and load of suspended bed sediment in a large river by means of acoustic Doppler technology, *J. Hydraul. Eng.*
Libicki, C., K. W. Bedford, and J. F. Lynch (1989), The interpretation and evaluation of a 3-Mhz acoustic backscatter device for measuring benthic boundary layer sediment dynamics, *J. Acoust. Soc. Am.*, *85*(4), 1501–1511.
Moate, B. D., and P. D. Thorne (2009), Measurements and inversion of acoustic scattering from suspensions having broad size distributions, *J. Acoust. Soc. Am.*, *126*(6), 2905–2917.
Moate, B. D., and P. D. Thorne (2012), Interpreting acoustic backscatter from suspended sediments of different and mixed mineralogical composition, *Cont. Shelf Res.*, *46*, 67–82.
Moore, S. A., J. Le Coz, D. Hurther, and A. Paquier (2013), Using multi-frequency acoustic attenuation to monitor grain size and concentration of suspended sediment in rivers, *J. Acoust. Soc. Am.*, *133*, 1959–1970.
Thorne, P. D., and D. Hanes (2002), A review of acoustic measurement of small scale sediment processes, *Cont. Shelf Res.*, *22*, 603–632.
Thorne, P. D., and D. Hurther (2014), An overview on the use of backscattered sound for measuring suspended particle size and concentration profiles in non-cohesive inorganic sediment transport studies, *Cont. Shelf Res.*, *73*, 97–118.
Thorne, P. D., and R. Meral (2008), Formulations for the scattering properties of suspended sandy sediments for use in the application of acoustics to sediment transport processes, *Cont. Shelf Res.*, *28*, 309–317.
Thosteson, E. D., and D. M. Hanes (1998), A simplified method for determining sediment size and concentration from multiple frequency acoustic backscatter measurements, *J. Acoust. Soc. Am.*, *104*(2), 820–830.
Topping, D. J., S. A. Wright, T. S. Melis, and D. M. Rubin (2007), High-resolution measurements of suspended sediment concentrations and grain size in the Colorado River in Grand Canyon using a multifrequency acoustic system, in *Proceedings of the 10th International Symposium on River Sedimentation*, vol. III, 470 pp., Moscow, Russia, 1–4 Aug.
Urick, R. J. (1948), The absorption of sound in suspensions of irregular particles, *J. Acoust. Soc. Am.*, *20*(3), 283–289.
Wright, S., D. Topping, and C. A. Williams (2010), Discriminating silt and clay from suspended sand in rivers using side-looking profilers, in *Proceedings of the 2nd Joint Federal Interagency Sedimentation Conference*, Las Vegas, Nev.